Granulite microfabrics and deformation mechanisms in southern Madagascar

Jean-Emmanuel Martelat [a,b,*], Karel Schulmann [c], Jean-Marc Lardeaux [a], Christian Nicollet [b], Hervé Cardon [a]

[a] *Laboratoire des Sciences de la Terre, V.C.B. Lyon I et ENS Lyon, UMR 5570, 46 allée d'Italie, 69364 Lyon, France*
[b] *Département de Géologie, Université Blaise Pascal, UMR 6224, 5 Rue Kessler, 63038 Clermont Ferrand, France*
[c] *Institute of Petrology and Structural Geology, Charles University, Albertov 6, Prague, Czech Republic*

Abstract

Optical microstructures and crystallographic preferred orientations were studied in naturally deformed granulite- to high-amphibolite facies quartzo-feldspathic rocks in southern Madagascar. The microstructures of coarse-grained granulite suggest that feldspar and quartz accommodated deformation by both dislocation and diffusion creep in the absence of melt. The extreme ductility of feldspar in dynamically recrystallized granulite is explained by activity of dislocation creep, in conjunction with stress-controlled intracrystalline diffusion.

In the studied rocks, the considerable volume of quartz is not interconnected even at high strain. The lack of its interconnectivity in coarse-grained granulites and in amphibolite facies granoblastic platy quartz rocks is explained by an extreme stability of the load-bearing framework structure at high-temperatures. In dynamically recrystallized granulite, the feldspar viscosity decreases so that quartz becomes enveloped by a weak feldspar matrix which inhibits its coalescence and interconnectivity.

We predict an important decrease in strength of quartzo-feldspathic granulites due to activity of diffusional creep and convergence of viscosity of recrystallized feldspar and quartz. © 1999 Elsevier Science Ltd. All rights reserved.

1. Introduction

Determination of deformation mechanisms in natural systems is complicated by the fact that the microstructures used as evidence reflect complex combination of metamorphic and deformational histories (White and Mawer, 1986). Therefore, one of the principal objectives of microstructural analysis is the identification of grain scale processes enabling the determination of deformation environment and mechanical properties of studied rocks.

Quartzo-feldspathic granulites are probably the most intensely studied polyphase rocks with respect to quartz textures (e.g. Sander, 1950; Behr, 1980). Most authors interpret quartz *c*-axis preferred orientations in granulites as a result of dislocation creep manifested by activity of the prism-[*c*] slip system (Lister and Dornsiepen, 1982). The activity of prism-[*c*] glide is also reported from partially molten rocks and from granites deformed at the solidus boundary (Blumenfeld et al., 1986).

Few microfabric studies explain crystallographic preferred orientation (CPO) of plagioclase as a result of dislocation motion on the (010)[001] and (010)[100] (Ji and Mainprice, 1988; Ji et al., 1988) at granulite facies conditions. Microstructures characteristic for dislocation creep in high-grade rocks have also been confirmed by several transmission electron microscope studies of naturally deformed plagioclase (e.g. Olsen

* Corresponding author.

E-mail addresses: jemartel@ens-lyon.fr (J.E. Martelat), schulman@prfdec.natur.cuni.cz (K. Schulmann), lardeaux@univ-lyon1.fr (J.M. Lardeaux), nicollet@opgc.univ-bpclermont.fr (C. Nicollet), hcardon@ens-lyon.fr (H. Cardon).
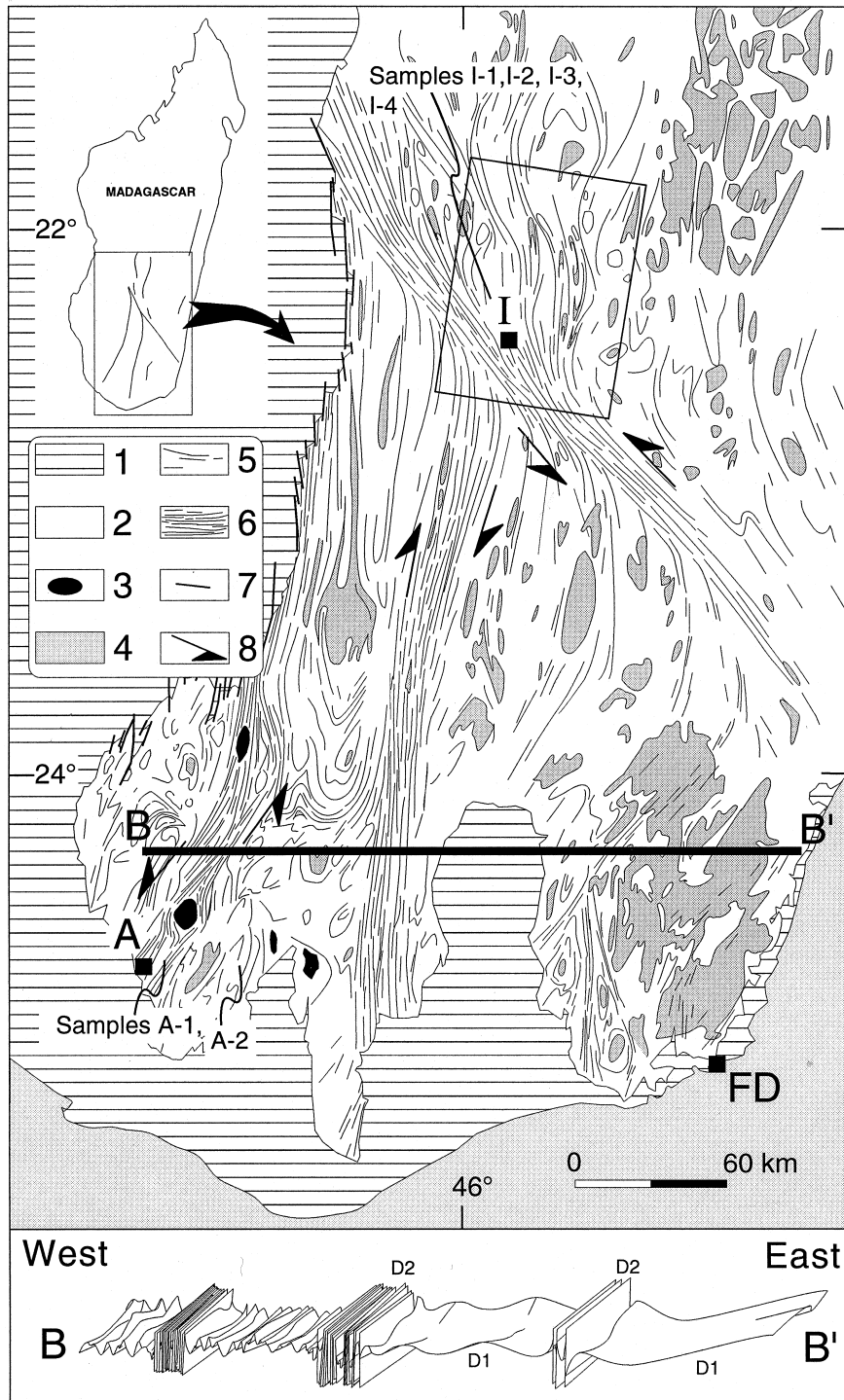
Fig. 1. Regional structural sketch map of the southern part of Madagascar. (1) Post-Cambrian sediments, (2) rocks equilibrated under granulite- and high-amphibolite facies conditions, (3) anorthosite, (4) granitoids, (5) foliation trends depicted from satellite images and field mapping, (6) shear zones, (7) major faults, (8) sense of shear. A schematic east–west cross-section is localized along the bold line (BB′). FD, I, A, towns of Fort-Dauphin, Ihosy and Ampanihy. The position of Fig. 2 and of the studied samples is indicated (I-1 to I-4, A-1 and A-2).

and Kohlstedt, 1984) and alkali feldspar (White and Mawer, 1986).

Diffusion-accommodated grain boundary sliding was described in very fine-grained quartzo-feldspathic high-

grade mylonites (Behrmann and Mainprice, 1987). In experimentally deformed quartzo-feldspathic rocks the diffusion creep is restricted to rocks with grain-size not exceeding 10 microns (Tullis, 1990). Diffusional creep

is also enhanced by presence of granitic melt (Dell'Angelo and Tullis, 1988).

The well-equilibrated microstructure of granulites is commonly interpreted by petrologists as a product of extensive solid state static annealing (Spry, 1969). Emphasis is placed on the geometric and morphological characteristics like the lack of like–like contacts between constituent minerals (Kretz, 1969, 1994; McLellan, 1983) and the presence of triple point junction network between constituent phases (Vernon, 1975).

Aspects of the microfabric such as the morphology of quartz–feldspar boundaries, grain indentations and grain overgrowths in coarse-grained quartzo-feldspathic high-temperature tectonites are rarely explained as the result of a combination of diffusion and dislocation creep processes (Gower and Simpson, 1992). Thus, diffusion creep of coarse-grained quartzo-feldspathic rocks is possible under natural melt-free amphibolite facies conditions.

From a purely mechanistic point of view, the quartzo-feldspathic granulite can be viewed as a polyphase mineralogical system consisting dominantly of K-feldspar and quartz. Handy (1990) applied a concept of strain and stress concentrations related to deformation of polyphase materials. According to this concept, the rocks form two types of structures: (1) a load bearing framework (LBF) structure in which the stress is concentrated in strong phases surrounding pockets of weak material; (2) an interconnected weak layer (IWL) structure marked by concentration of stress and deformation in weak minerals forming an interconnected phase. As indicated by experiments, progressive deformation leads to the breakdown of LBF structure which becomes unstable at higher strain values (Jordan, 1987). It gives rise to a so-called 'banded structure' marked by alternations of monomineralic layers which was also reported from naturally deformed quartzo-feldspathic rocks under amphibolite facies conditions (Schulmann et al., 1996). However, in quartzo-feldspathic granulites such a banded structure does not develop. This can be interpreted as an effect of post-tectonic annealing or as a result of stability of LBF structure under high-temperature conditions due to diffusion creep.

In this paper we discuss the significance of rock fabrics and microstructures of the Madagascar lower crust coeval with granulite- to higher-amphibolite facies metamorphism. Microstructural- and fabric analysis were performed in quartzo-feldspathic rocks in order to identify a creep regime under high-temperature conditions. The microstructural study is compared with extrapolated rheological laboratory data in order to establish the strength of the studied granulites.

2. Regional framework

The Madagascar basement forms a part of Gondwanaland that separated from the other segments during Mesozoic rifting. The structures in this basement are related to the Mozambique belt which is a major Pan-African continental collision zone (Shackleton, 1986). The southern part of Madagascar (Fig. 1) consists of Early Precambrian (Caen-Vachette, 1979) continental crust strongly reworked during Pan-African times (600–530 My, Andriamarofahatra et al., 1990; Paquette et al., 1994). Contrasting lithologies that have been mapped include: orthogneisses, high-grade paragneisses, marbles, granitoids, metabasites and anorthosites (Besairie, 1970).

Numerous petrological studies provide evidence for regional Pan-African granulite facies metamorphism in southern Madagascar (see reviews in Nicollet, 1990; Windley et al., 1994). Mafic granulites are composed of cpx + opx + pl + brown amp + grt + qtz + ilm and rt. In few places sapphirine and corundum-bearing amphibolites have also been reported. Migmatite paragneisses consist of qtz + kfs + grt + pl + sil ± crd ± bt and rare grandidierite. Aluminous residues are rich in bt + crd + grt or sil and more rarely sapphirine and kornerupine (Nicollet, 1990). Quartzo-feldspathic granulites are abundant and are composed of qtz + kfs + pl + grt ± sil ± spl. Quantitative temperature and pressure estimates have been obtained for reactions involving cpx + opx + grt + amp + qtz + pl mineral assemblage in mafic lithologies (Martelat et al., 1997), grt + spl + qtz or grt + crd assemblages in metapelites (Moine et al., 1985; Nicollet, 1985, 1990). These different techniques yield consistent temperature estimates at around $750 \pm 50°C$. The peak pressure estimates show a systematic increase from 0.4 GPa in the east towards 1 GPa in more western parts of the island.

3. Structural evolution

Two major Pan-African deformation events have been recognized in southern Madagascar: the first (D_1) is represented by a planar granulitic foliation, isoclinal folds and an E–W-stretching lineation (Martelat et al., 1997). The second (D_2) corresponds to the development of vertical shear zones and refolding of D_1 fabrics (Fig. 1) attributed to a major compressional phase (Martelat et al., 1997). The shear zones separate regions of weaker D_2 deformation characterized by folding of earlier metamorphic fabrics with refolding intensity increasing westwards.

The style of deformation in the domains between shear zones is characterized by a granulite facies foliation (S_1) represented by compositional banding, planar arrangement of platy minerals and flattening of
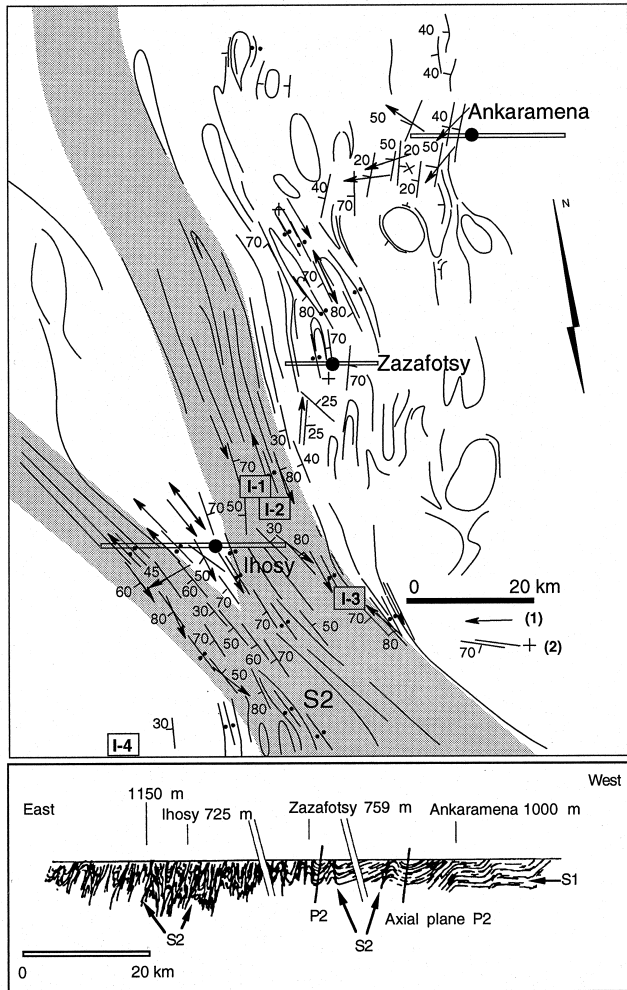
Fig. 2. Example of the sampling strategy across the kilometre scale shear zone near the town of Ihosy (I-1 to I-4). (1) Mineral stretching lineations L_1 and L_2, (2) foliations S_1 and S_2. The grey area marks major D_2 shear zones. A schematic east–west cross-section at the bottom of the figure shows the relationship between D_1 and D_2 structures. The cross-section is constructed using local cross-sections (double line) passing through the towns of Ihosy, Zazafotsy and Ankaramena.

and planar arrangement of granulite facies minerals and by the compositional banding of pyroxene-bearing and feldspar-rich bands. In quartzo-feldspathic granulites, the L_2 lineation is locally marked by alignment of grt, spl, qtz and sil.

4. Rocks studied in outcrop

We have studied quartzo-feldspathic granulites because of their simple mineralogy characterized by an average modal composition 50% K-feldspar, 40% quartz and 7% plagioclase. Other minerals occupy less than 3% of the rock.

Sampling was carried out along two cross-sections perpendicular to two main vertical D_2 shear zones (Ihosy and Ampanihy) and covering adjacent regions with D_1 subhorizontal fabrics (Fig. 2). The first group of granulite samples was collected at outcrops characterized by flatlying D_1 foliation and E–W-trending L_1 lineation. The mineral assemblage of samples A-2 and I-4 is marked by the presence of kfs, pl, qtz, green spl, (ZnO or $Cr_2O_3 < 0.1$ wt%), grt (alm 50–75%, prp 19–38%) $\pm$ sil and rt. Scarce tiny secondary biotite grains are developed at garnet rims. The second group of samples I-3, I-1, I-2 and A-1 was collected at outcrops within D_2 shear zones marked by a vertical foliation and subhorizontal lineation (Fig. 2). Sample I-3 is characterized by a mineral assemblage similar to that of the first group but with a higher modal amount of grt and sil. The samples I-1, I-2 and A-1 contain qtz, pl, mc, bt, ilm $\pm$ grt $\pm$ sil. Therefore, we regard these last three samples as quartzo-feldspathic granulites partly reequilibrated under amphibolite facies conditions.

5. Microstructures

The microstructural characteristics of grain size, grain shape, geometry of grain boundaries, and grain contact frequency were systematically studied. The microstructural work was enhanced by the study of crystallographic preferred orientation of K-feldspar and quartz. Three principal types of microstructures were recognized: Preserved D_1 fabrics outside the shear zones (Type 1), partly recrystallized granulite (Type 2) and D_2 reequilibrated granulite (Type 3).

5.1. Type 1 fabrics in granulite (A-2, I-4 outside the shear zone)

The samples show a typical granulitic microfabric in which mesoperthitic alkali feldspar forms an interconnecting phase enclosing all other mineral phases. Mesoperthitic alkali feldspar is mostly present in the

quartz ribbons and feldspar aggregates. This foliation displays subhorizontal stretching and a mineral lineation defined by an E–W alignment of granulitic minerals. It is locally refolded by synfolial, rootless folds with hinges parallel to the regional stretching lineation.

The D_2 deformation within the blocks separated by shear zones is characterized by F_2 folding of all previous structures and results in the development of Type 2 interference fold patterns (mushroom of Ramsay, 1967) on all scales. These folds are open to tight with subhorizontal N–S-trending hinges and steep axial planes. In contrast, the F_2 folds within D_2 shear zones are isoclinal with steep axial planes and subhorizontal or subvertical fold hinges. The planar fabric within the shear zones is defined by flattening
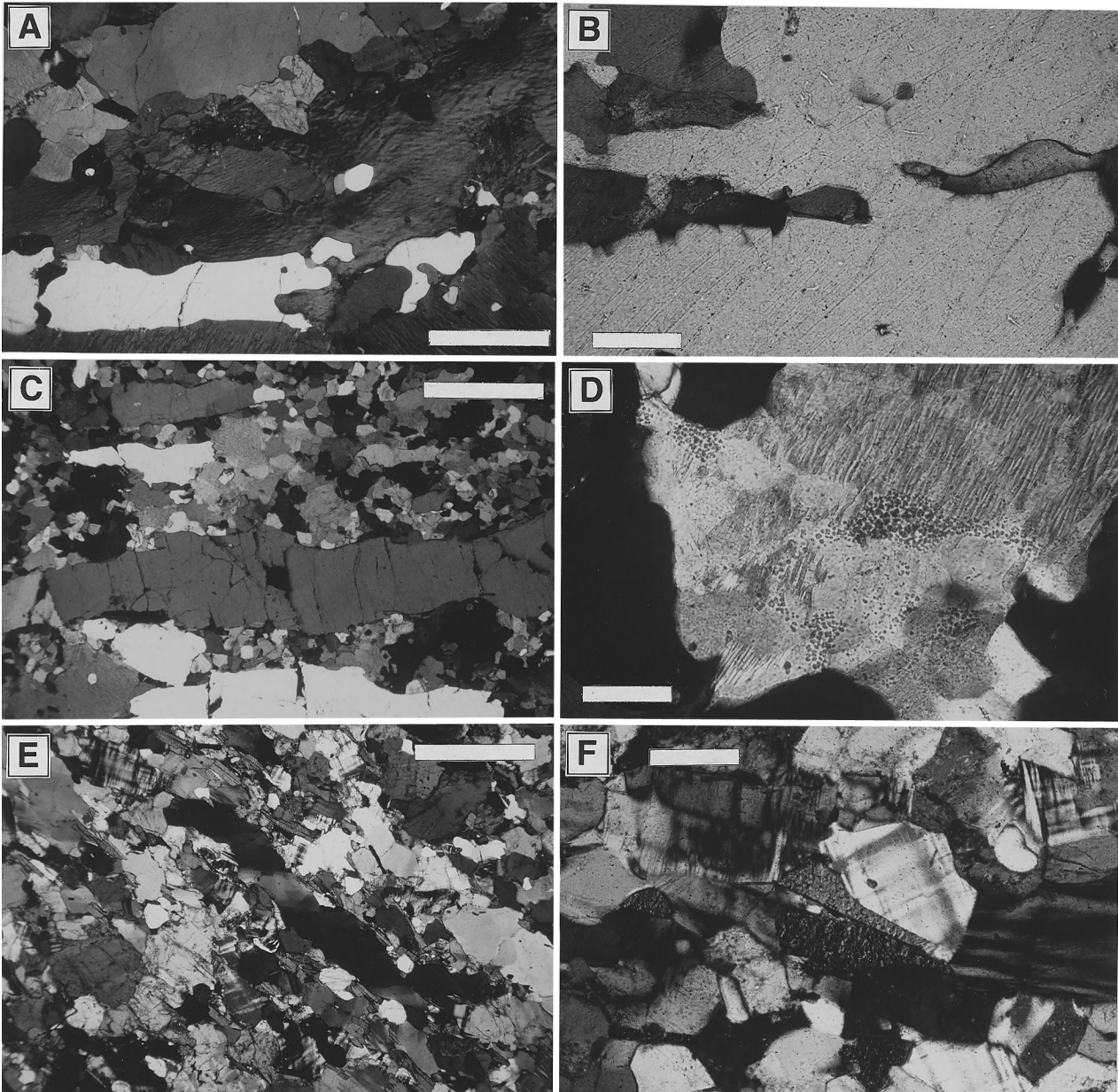
Fig. 3. Micrographs of representative quartzo-feldspathic granulites. (a) and (b) D_1 granulite microfabrics in XZ section of the strain ellipsoid; (c–f) D_2 granulite microfabrics in XZ section of the strain ellipsoid. (a) Elongate mesoperthitic K-feldspar encloses monocrystalline quartz ribbons. Note cusp at K-feldspar–quartz boundary parallel to the foliation (scale bar 1 mm). (b) Cusp of K-feldspar included in quartz (scale bar 200 μm). XZ section of strain ellipsoid. (c) Recrystallized alkaline feldspar surrounding monocrystalline quartz ribbons (scale bar 1 mm). (d) Recrystallization of alkaline feldspar by compositionally and crystallographically controlled sub-grain rotation. New grains are discrete plagioclase or K-feldspar (scale bar 200 μm). (e) Type 3 fabric, matrix composed by subequant grains of plagioclase and microcline and biotite. Quartz forms strained monocrystalline ribbons (scale bar 1 mm). (f) Detail of triple point network in microcline–plagioclase matrix (scale bar 200 μm).

form of sub-equant grains of irregular shape ranging from 0.5 to 4 mm in size. Locally the grains reach 3 mm in length and are elongate with aspect ratio up to 5:1 (Figs. 3a and 4a). The grain boundaries of sub-equant grains are straight and often meet in triple point junctions. Large feldspar crystals show lobate mutual boundaries.

Quartz is present in the form of large elongate monocrystalline ribbons up to 3 mm long and 0.5–2 mm wide or as thick polycrystalline aggregates (Figs. 3a and 4a). Quartz often includes small grains of K-feldspar and plagioclase (Fig. 3b). It also occurs as irregular polycrystalline aggregates with strongly sutured grain boundaries. The most characteristic
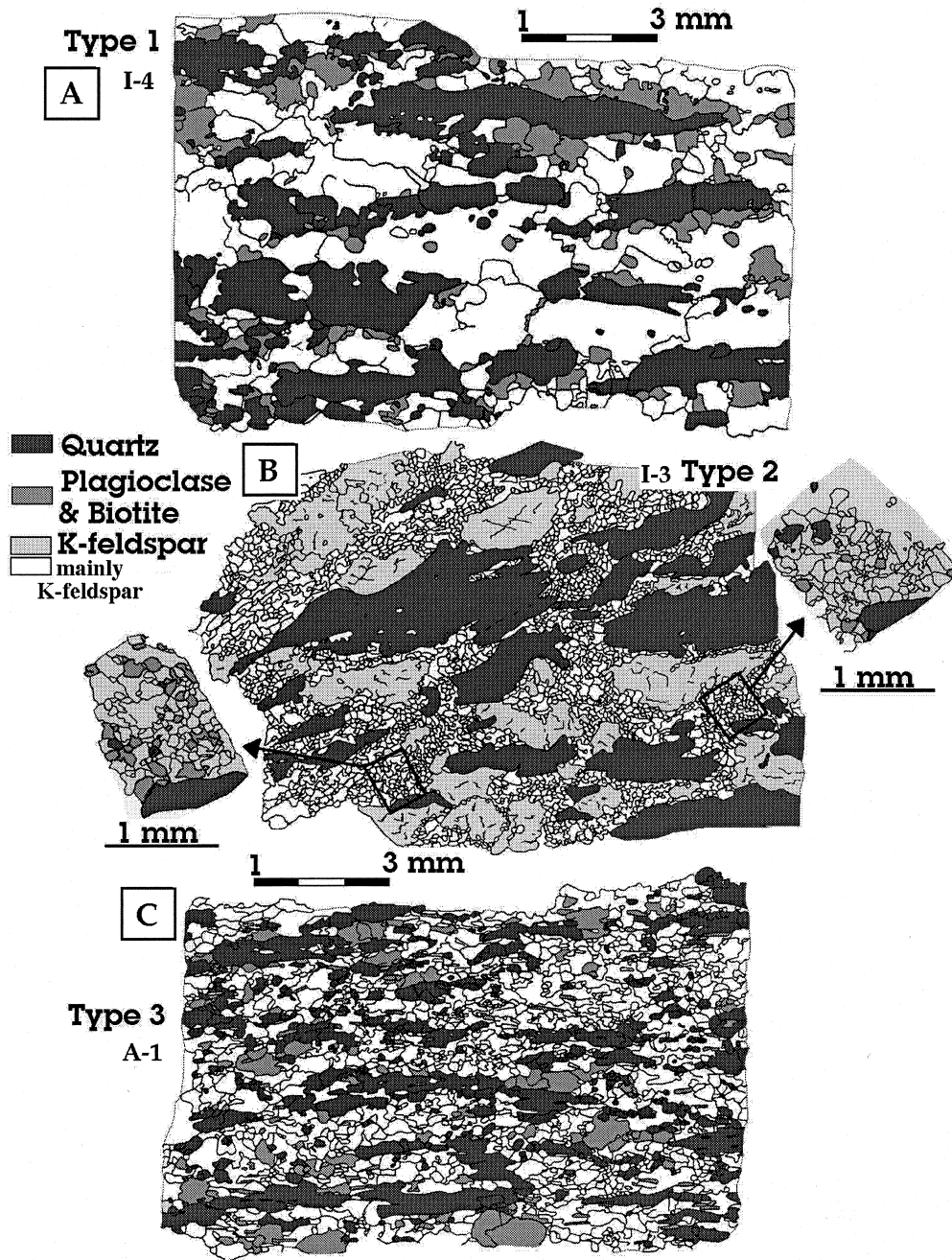
Fig. 4. Maps of thin sections of granulite microfabrics (*XZ* sections of the strain ellipsoid). (a) Coarse grained Type 1 fabric (I-4 sample). (b) Type 2 fabric, inset shows details of composition of fine grained matrix (I-3 sample). (c) Type 3 fabric with elongated quartz ribbon (A-1 sample).

intracrystalline microstructures are prismatic subgrain boundaries parallel to ribbon elongation or a rectangular chess-board microstructure indicating the presence of both basal and prismatic subgrain boundaries (Kruhl, 1996). Quartz–feldspar boundaries are gently curved showing cusps pointing from feldspar to quartz fields. The cusps in sections perpendicular to the foliation trend mostly parallel to the foliation. Two types of quartz–feldspar phase boundary cusps have been identified in thin sections similar to those described by Gower and Simpson (1992): long cusps at the terminations of feldspar promontories pointing into quartz
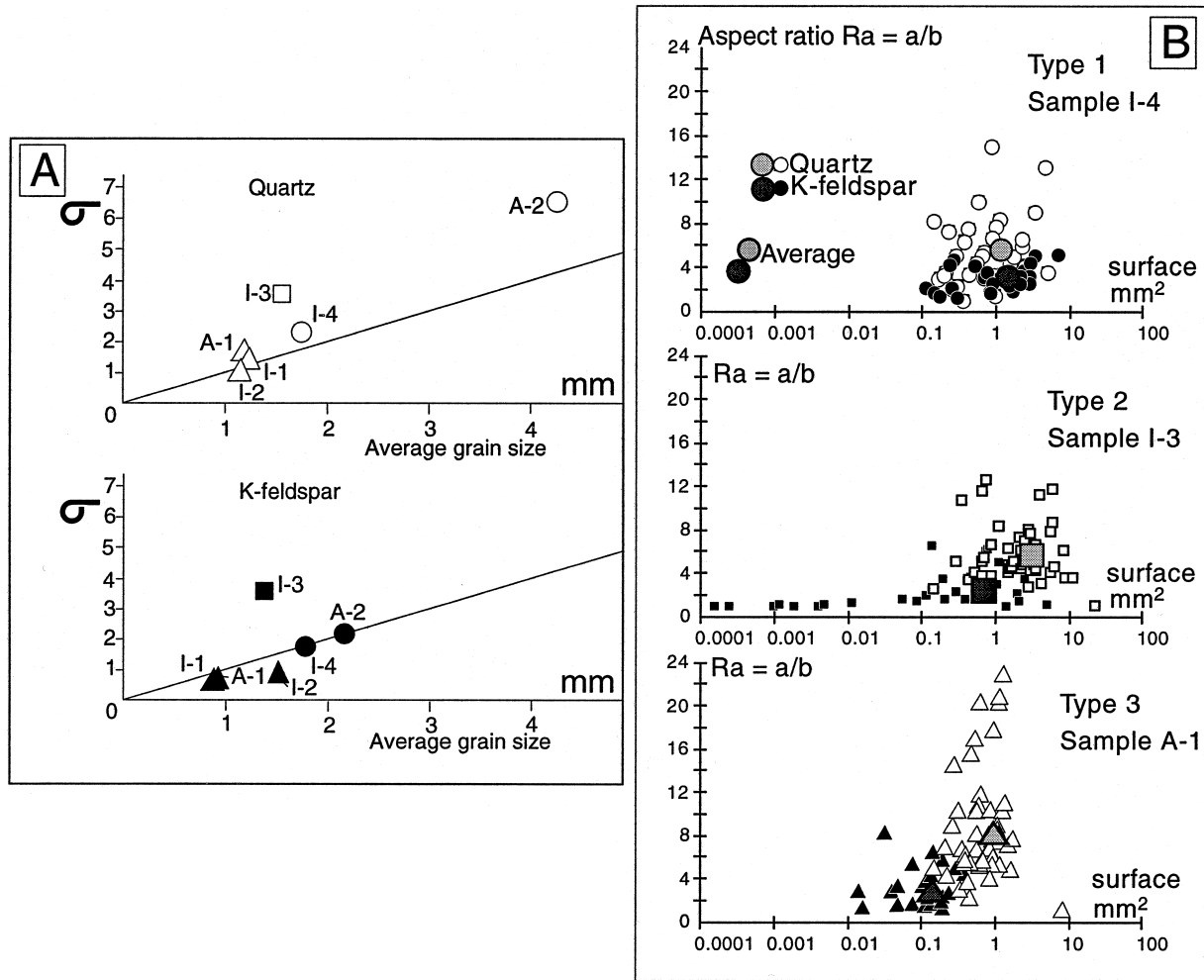
Fig. 5. Results of grain-size and of grain aspect ratio analyses. (a) Orthogonal plot of average grain-size vs grain-size spread calculated as standard deviation (σ). (b) Orthogonal plot of grain-size surface (mm^2) vs grain aspect ratios ($R_a = a/b$) for quartz and feldspar. Long axis a and short axis b are measured in XZ sections. Large symbols indicate average grain-size and aspect ratio. Circle, square and triangle correspond to Type 1, Type 2 and Type 3 fabrics, respectively.

fields (Fig. 3a), and foliation parallel cusps developed at the termination of feldspars enveloped in quartz (Fig. 3b).

5.2. Type 2 fabrics (I-3 sample inside shear zone)

The main deformation feature is intense dynamic recrystallization of large alkali feldspar crystals leading to grain-size reduction (Figs. 3c and 4b). Relicts of mesoperthites show a core-and-mantle structure (White, 1976) marked by elongate subgrain walls in the core and sub-equant subgrains (0.2–0.5 mm) at their margins. The least deformed alkali feldspars show well preserved mesoperthitic structures (Fig. 3d). There is a compositional and crystallographic control of subgrain formation similar to that observed by White and Mawer (1986, Fig. 3d). This involves devel-

opment of discrete K-feldspar and plagioclase subgrains associated with progressive misorientation of subgrain boundaries. Continued deformation leads to dynamic recrystallization by subgrain rotation producing separated K-feldspar and plagioclase new grains. At least 50% of the sample consists of a recrystallized groundmass composed of small sub-equant K-feldspar and plagioclase grains.

Quartz forms elongate monocrystalline ribbons up to 7 mm in length and 1–2 mm in width, and does not show signs of dynamic recrystallization. The typical internal feature is chess-board undulatory extinction or prism subgrain boundaries oriented obliquely to ribbon margins (Fig. 3c). Boundaries between quartz and K-feldspar are gently curved and exhibit cusps of recrystallized feldspar fields pointing into quartz parallel to the foliation trend (Fig. 4b).
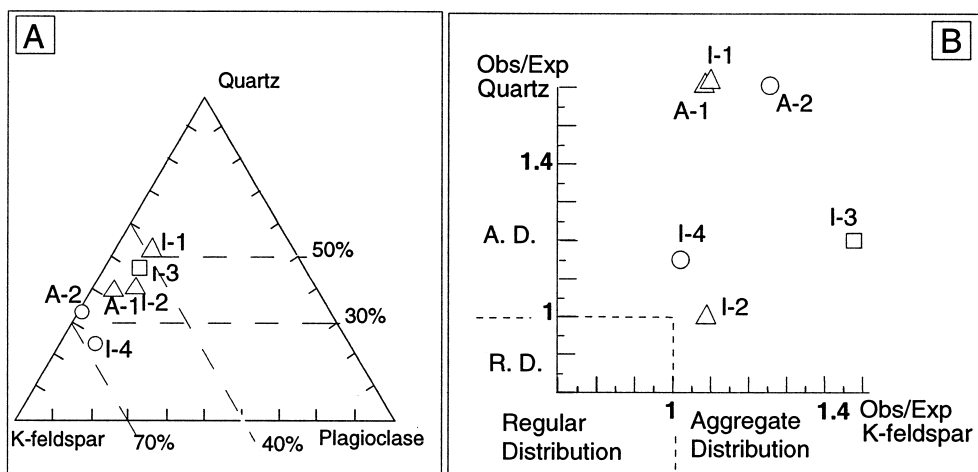
Fig. 6. Modal composition and results of grain contact frequency analysis for quartzo-feldspathic granulites. (a) Modal composition of quartzo-feldspathic granulites used for quantitative textural analysis is plotted in the quartz–plagioclase–K-feldspar triangle. (b) Orthogonal plot of observed/expected frequencies from quartzo-feldspathic granulites. The expected values are calculated after McLellan (1983). Circle, square and triangle correspond to Type 1, Type 2 and Type 3 fabrics, respectively.

5.3. Type 3 fabrics (samples I-1, I-2 and A-1 inside the shear zone)

The rock exhibits an equigranular microstructure of matrix surrounding strongly elongated platy quartz. The foliation is emphasized by a shape preferred orientation of small biotites and by quartz ribbons (Figs. 3e and 4c). The fine-grained matrix is composed mostly of small grains of K-feldspar reaching 0.5 mm in size. The grains have flattened shapes and well-equilibrated straight boundaries (Fig. 3f). Abundant microcline twinning is developed both in the rare relictual clasts and in almost all new grains. K-feldspar locally shows an untwinned core surrounded by twinned microcline.

Quartz occurs in the form of highly elongated monocrystalline ribbons (Figs. 3e and 4c) which show strong undulatory extinction and numerous prismatic subgrains oblique to ribbon margins.

6. Quantitative fabric analysis

This fabric analysis is based on a statistical evaluation of grain-size distributions and grain boundary frequencies (McLellan, 1983; Kretz, 1994). The grain-size of dynamically recrystallized mineral aggregates is controlled by the rate of subgrain rotation (N) and by the rate in which grains are consumed by grain boundary migration (G) (Hickey and Bell, 1996). Grains undergo diminution where average $N/G > 1$, preservation of grain-size where $N/G = 1$ and increase in grain-size where $N/G < 1$. The N/G ratio is controlled by the strain rate/temperature ratio ($\dot{e}/T$), so that decreasing $\dot{e}/T$ leads to an increasing role of grain boundary migration and increasing $\dot{e}/T$ enhances sub-

grain rotation. Grain boundary frequency is dependent on grain boundary energy (Vernon, 1975) which is also controlled by temperature and strain rate.

6.1. Grain-size statistics and grain aspect ratio

Grain-size statistics play an important role in the identification of static grain growth during post-tectonic annealing (Bons, 1993) and in the study of fabric evolution during dynamic recrystallization. A distinction needs to be found between dynamic recrystallization associated either with syntectonic grain growth and grain shrinkage by migration of grain boundaries (Urai et al., 1986), or with overall grain-size reduction by rotation recrystallization. The size of grains has been measured using a line intercept method of Kretz (1994). The results of grain-size analyses are presented in the form of diagrams of average grain-size vs standard deviation (Fig. 5a). The grain-size was also plotted as a function of grain aspect ratio for both minerals (R_a, Fig. 5b).

The grain-size distribution of quartz for Type 1 fabrics in Fig. 5 is consistent with the presence of large quartz ribbons and numerous small interstitial quartz grains. K-feldspars exhibit smaller average grain-size than quartz, and also a significantly smaller grain-size spread which is explained by relatively uniform grain-size distribution of well-equilibrated K-feldspar mosaics. In the Type 2 fabrics, quartz exhibits a smaller average grain-size than in the previous granulite type. The K-feldspar shows bimodal grain-size distribution characterized by the presence of coarse relictual clasts that range from 0.1 to 3 mm and a large number of small recrystallized grains below 0.1 mm in size (Fig. 5b). This grain-size distribution is marked by a

small average grain-size as well as by a relatively large spreading in grain-size (Fig. 5a). The samples of Type 3 fabrics show small average grain-size of quartz (average size = 1 mm) and K-feldspar (average size = 0.3 mm). K-feldspar exhibits a clear predominance of very small grains with a small average grain-size and also small spreading in grain-size.

The Type 1 fabric exhibits similar values of average grain-size and high average grain aspect ratio, R_a, for both K-feldspar ($R_a = 3$) and quartz ($R_a = 6$) indicating that the whole aggregate is composed of grains with rather large size and similar elongation (Fig. 5b). The partially recrystallized Type 2 fabric shows the very small aspect ratio of small recrystallized K-feldspar grains ($R_a < 1.5$), and the higher aspect ratio of relict large clasts ($R_a > 3$). Large quartz clasts are more elongated than relict feldspars and have slightly smaller average aspect ratio ($R_a = 5$) than quartz of the Type 1 fabric (Fig. 5b). The Type 3 fabric exhibits weak elongation $R_a = 2$ of small recrystallized feldspar grains and high average aspect ratio of quartz ribbons corresponding to $R_a = 8$ (Fig. 5b).

6.2. Grain contact frequency analysis

A grain contact frequency analysis was developed to quantify the microstructural mineral relationships (Flinn, 1969). The line-intercept method was used to examine deviations of contact relationships between individual phases from random distribution (Kretz, 1969). There are two possible deviations from grain contact random distribution: (1) an aggregate distribution implying predominance of contacts of the same minerals, and (2) a regular distribution in which contacts between different phases are more common (McLellan, 1983). The former grain contact distribution is characteristic of solid state differentiation associated mostly with dynamic recrystallization of mineral phases. Indeed, deformations of quartzo-feldspathic rocks under amphibolite facies conditions lead to coalescence of monomineral aggregates derived from recrystallized grains (Schulmann et al., 1996). On the other hand, regular grain contact distribution is commonly interpreted as resulting from solid state annealing under very high-temperatures (McLellan, 1983).

The results of grain contact frequency analyses are presented in a diagram displaying ratios of observed and expected grain contact frequencies for K-feldspar and for quartz which represent the most abundant mineral phases in studied samples (Fig. 6a, b). The expected and observed values have been calculated using the method of McLellan (1983). The resulting plot shows very weak aggregate or almost random distribution of large K-feldspar grains of samples A-2 and I-4 of coarse-grained Type 1 fabric. The

aggregate distribution is slightly better pronounced in partly recrystallized K-feldspar of sample I-3 (Type 2 fabric), and develops towards random distribution in Type 3 fabric (samples A-1, I-1 and I-2). Quartz shows slightly higher aggregate patterns which could however be influenced by contrasting grain-sizes and small modal amount volume fractions.

6.3. The interpretation of quantitative microfabric analysis

In the Type 1 fabric, the large grain-size and uniform size distribution of K-feldspar and its weak aggregate distribution with few like–like contacts indicates weak solid state differentiation accompanied by solid state annealing. However, the regular distribution commonly described in statically annealed granulites (Kretz, 1969) is not achieved. The large average grain-size of both the quartz and feldspar is interpreted as the result of a high grain boundary migration rate (G) with respect to the rate of subgrain rotation recrystallization N at a small $\dot{e}/T$ ratio (Hirth and Tullis, 1992).

The subgrain rotation recrystallization of K-feldspar in Type 2 fabric leads to development of heterogeneous grain-size distribution and increasing degree of aggregate distribution of K-feldspar (Fig. 6b). This process is connected with solid state differentiation and an increase in total surface energy of the feldspar aggregate. The $\dot{e}/T$ ratio increased at this stage such that average $N/G > 1$ and the initial large grain size of feldspar cannot be preserved. Even if the driving force for grain boundary migration was still high, the new grains were produced at such a rate of subgrain rotation N that the average grain size was significantly reduced. Weak aggregate distribution is interpreted as a result of compositional control of the dynamic recrystallization process leading to heterogeneous nucleation of K-feldspar and plagioclase at the expense of original mesoperthitic feldspars.

The grain contact frequency distribution in the Type 3 fabric shows an almost random pattern corresponding to an equidimensional and randomly distributed feldspar aggregate. High-temperature (amphibolite facies conditions) is held responsible for reequilibration of the equigranular microstructure associated with only slight grain growth and rearrangement of grain boundaries to a triple point network. Larger grain-sizes of the feldspar mosaic of mylonitic samples with respect to Type 2 granulite can be explained by a decrease in $\dot{e}/T$ ratio on a local scale such that the average $N/G < 1$ is inducing more important grain boundary migration.
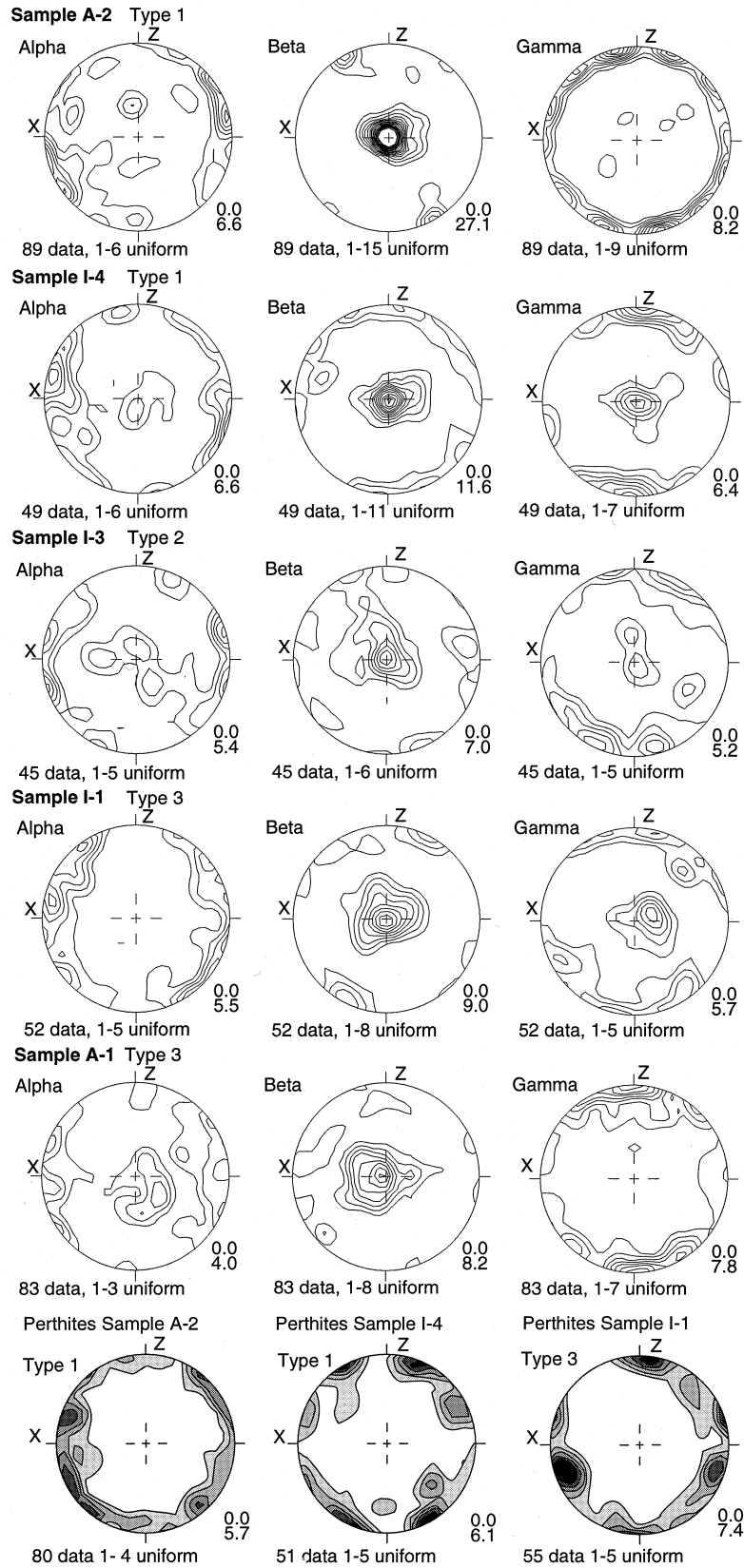
Fig. 7. Crystallographic preferred orientations of alkali feldspars for optical directions α, β and γ of Type 1 fabric (samples I-4, A-2); Type 2 fabric (sample I-3), and of Type 3 fabric (samples I-1, A-1). Fabrics are measured in *XZ* sections of the strain ellipsoid. Lower hemisphere equal area projection. Diagrams contoured at multiples of uniform distribution (from I-15 to I-3 uniforms). The foliation normal is vertical, and the stretching lineation is horizontal. At the bottom of the figure are pole orientation diagrams of the perthitic walls from the samples (A-2, I-4, I-1). Lower hemisphere equal area projection. Diagrams contoured at multiples of uniform distribution.

Plan YZ

Sample I-4 Type 1
190 data 1, 2 , 3 times uniform
0.0
4.3

Sample I-3 Type 2
160 data 1, 2 , 3 , 4 times uniform
0.0
3.9

Sample A-1 Type 3
200 data 1, 2, 3, 4 times uniform
0.0
4.5

Plan XZ

Sample I-4 Type 1
199 data 1, 2 , 3 times uniform
0.0
4.1

Sample A-2 Type 1
116 data 1, 2, 3 times uniform
0.0
3.3

Sample I-3 Type 2
122 data 1, 2 , 3 , 4 times uniform
0.0
3.3

Sample I-1 Type 3
114 data 1, 2, 3 times uniform
0.0
3.6

Sample A-1 Type 3
199 data 1, 2, 3, 4 times uniform
0.0
3.9

Sample I-2 Type 3
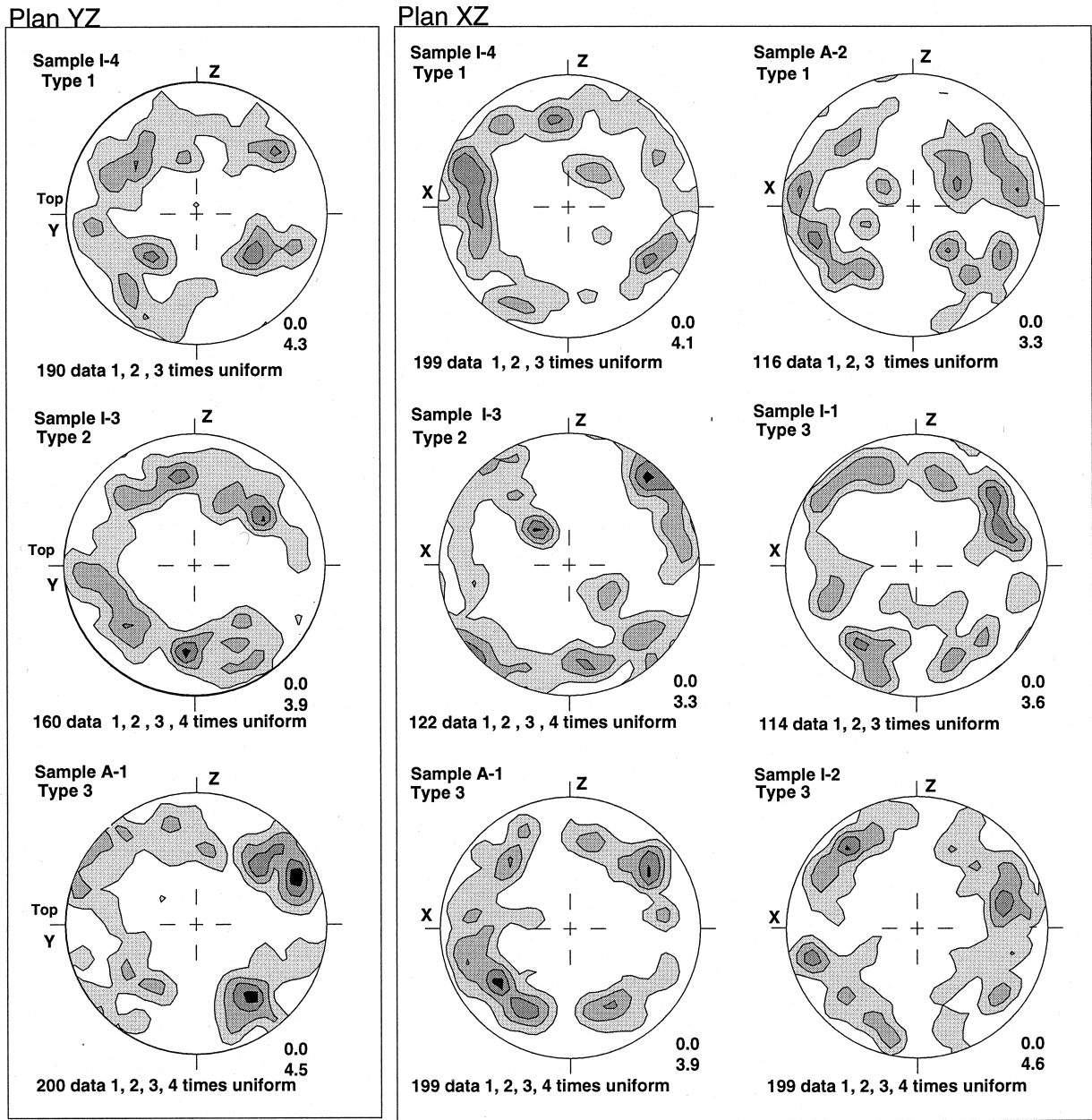199 data 1, 2, 3, 4 times uniform
0.0
4.6

Fig. 8. Orientation diagrams of quartz *c*-axes from quartzo-feldspathic granulites (Type 1 fabric, samples I-4, A-2; Type 2 fabric, sample I-3 and Type 3 fabric, samples I-1, I-2, A-1). Lower hemisphere equal area projection (*XZ* and *YZ* sections of strain ellipsoid). Diagrams contoured at multiples of uniform distribution.

7. Crystallographic preferred orientations of K-feldspar and quartz

The complete optical indicatrix of K-feldspar and the orientation of *c*-axes of quartz were measured using a Universal Stage in six samples covering all microstructural varieties. We assume that the mineral lineation corresponds to the *X* axis and the grain shape foliation to the *XY* plane of finite strain ellipsoid.

7.1. K-feldspar

The orientation of the optical indicatrices α, β, γ has been measured on 50 grains for each of the six samples. As K-feldspar is a monoclinic mineral there is not a simple relationship between optical directions and crystallographic axes. Hence, γ coincides with the normal to (010) (pole of the largest crystal face), α lies at an angle of 5° with respect to the [100] direction

(mineral elongation) and β forms an angle of 20° with the [001] direction.

The feldspars in all samples exhibit a strong optical fabric despite different tectonic environments. Type 1 fabrics outside the shear zones (Fig. 7, sample A-2, I-4) can be described as follows: β forms a strong maximum perpendicular to mineral lineation and parallel to foliation (Y finite strain axis), α axes are distributed along a girdle in the XZ plane with a strong maximum oblique to lineation. The γ axes form either a girdle in the XZ plane with pronounced maxima oblique to the Z axis, or one strong maximum parallel to the Y axis of the fabric ellipsoid. The orientation of perthitic walls has been measured in large feldspar grains which generally contain α and β optical directions (Fig. 7).

In Type 2 fabric (Fig. 7, sample I-3), two generations of grains occur: host grains and recrystallized new grains. The orientation diagram for the host and recrystallized new grains reveal similar crystallographic orientations. β forms a strong maximum parallel to the Y axis and several small sub-maxima in the XZ plane. The γ axes are distributed mostly in the XZ plane and form two maxima slightly asymmetrical with respect to the pole of the foliation.

The α, β and γ orientations in Type 3 fabrics (Fig. 7, samples I-1, A-1) are generally similar to those of granulites outside the shear zones. The main difference is expressed by γ axes orientations which plot either around the Y axis of finite strain or near the pole of the foliation. The β axis distributions are also alternating around Y and Z axes.

7.2. Quartz

The quartz c-axis preferred orientation was measured in large monocrystalline ribbons as well as in small grains in sections parallel to the lineation and perpendicular to the foliation (XZ) and in sections perpendicular to the foliation and lineation (YZ). In samples I-4 and A-2 of Type 1 fabrics, maxima occur close to the foliation and along the lineation (Fig. 8). The most typical pattern of Type 2 and Type 3 fabrics are maxima symmetrically distributed with respect to the XY plane, and forming an angle of less than 40° with the foliation. The angle between maxima and the XZ plane varies between 10 and 30°. Subordinate maxima close to the foliation plane also occur. The patterns measured in YZ planes of representative samples confirm the quartz c-axis distribution measured in XZ sections.

7.3. Possible slip systems in K-feldspar and in quartz

The preferred orientation of the optical indicatrix of feldspars can be used as an indirect indicator of active slip systems in natural tectonites (Ji et al., 1988).

Consequently, the concentration of γ parallel to the pole of the foliation plane is indicative of slip on the (010) plane, and weaker maxima normal to foliation may indicate subordinate slip on (001). Optical directions α and β coincide with the direction of perthite planes which acted as planes of preferred slip. The γ direction coincides with (010) planes in the case of K-feldspar, and therefore an obliquity of γ maxima with respect to the pole of the foliation could be used as a potential kinematic indicator (Ji et al., 1988). Moreover, the weak asymmetry of orientations of perthite walls, generally parallel to (010) planes and associated with the stable orientation of the optical indicatrix, indicates a non-coaxial flattening regime consistent with mesoscopic shear criteria. The strong concentration of α close to the mineral lineation is entirely consistent with slip in the [100] direction in all studied samples. Experimental studies have shown that at 700°C samples oriented parallel to (010)[100] slip systems were weaker than others (Tullis, 1983).

A quartz c-axis distribution close to the mineral lineation (samples I-4, A-2) is commonly attributed to the activity of prism-[c] slip (Mainprice et al., 1986). The maximum oblique to the mineral lineation is interpreted as a result of non-coaxial deformation and still active prism-[c] slip. c-Axis orientations with two maxima at 35–40° positions to the elongation lineation (I-3, A-1, I-2) indicate an opening angle higher than 100°, reported from granulite facies rocks (Sander, 1950). In agreement with Kruhl (1996), we suppose that the observed texture pattern corresponds to a high activity of prism-[c] slip accommodating coaxial deformation of plane strain symmetry. The prism-[c] slip system is generally reported from granitoids deformed at the solidus boundary (Gapais and Barbarin, 1986) and from granulite facies tectonites (Lister and Dornsiepen, 1982; Kruhl, 1996). However, Garbutt and Teyssier (1991) argue that prism-[c] glide may occur under amphibolite facies conditions if hot water-rich fluids are present which would explain the quartz c-axis patterns in samples of the Type 3 fabrics.

8. Discussion

8.1. Deformation mechanisms

The Type 1 fabric is marked by the presence of large grains and well-equilibrated boundaries between adjacent K-feldspar grains suggesting high-temperature thermal equilibration. The feldspar–quartz boundaries are characterized by feldspar cusps parallel to foliation traces. This microstructure is interpreted to have resulted from migration assisted by diffusional creep, a process called dynamic recrystallization of quartz–feldspar boundaries by Gower and Simpson (1992). This

Table 1
Variations of creep strength and viscosity of plagioclase and quartz with temperature. Columns 2 and 3 represent calculated values of σ using equation 5 of Handy (1994) for a strain rate $\dot{e} = 10^{-14}$ s^{-1}. Rheological parameters for quartzite from Jaoul et al. (1984) and for albitic feldspar from Shelton and Tullis (1981). Columns 4 and 5 represent viscosities of quartz and albitic feldspar and column 6 viscosity ratio μ_{pl}/μ_{qtz} (R. viscosity)

Temp. (°C)	σ Plagioclase (MPa)	σ Quartz (MPa)	Plagioclase viscosity (Pa s^{-1})	Quartz viscosity (Pa s^{-1})	R. viscosity, μ_{pl}/μ_{qtz}
600	1154.69	97.32	5.77×10^{22}	4.87×10^{21}	11.86
650	458.07	35.75	2.29×10^{22}	1.79×10^{21}	12.81
700	207.38	15.15	1.04×10^{22}	7.57×10^{20}	13.69
750	104.35	7.20	5.22×10^{21}	3.60×10^{20}	14.50
760	91.95	6.28	4.60×10^{21}	3.14×10^{20}	14.65
770	81.29	5.49	4.06×10^{21}	2.75×10^{20}	14.80
780	72.09	4.82	3.60×10^{21}	2.41×10^{20}	14.95
790	64.13	4.25	3.21×10^{21}	2.12×10^{20}	15.10
800	57.21	3.75	2.86×10^{21}	1.88×10^{20}	15.24
810	51.19	3.33	2.56×10^{21}	1.66×10^{20}	15.38
820	45.92	2.96	2.30×10^{21}	1.48×10^{20}	15.52
830	41.30	2.64	2.07×10^{21}	1.32×10^{20}	15.66
840	37.25	2.36	1.86×10^{21}	1.18×10^{20}	15.80
850	33.67	2.11	1.68×10^{21}	1.06×10^{20}	15.93

grain boundary migration results from diffusive mass transfer along phase boundaries. The K-feldspar preferred orientation pattern is consistent with (010)[100] slip and quartz texture suggests the activation of prism-[c] slip. Both types of feldspar and quartz textures are compatible with high-temperature conditions of ductile deformation (Lister and Dornsiepen, 1982; Tullis, 1983). Quantitative microstructural analysis and analysis of crystallographic preferred orientations of K-feldspar and quartz suggest dislocation creep accompanying diffusional mass transfer as main deformation mechanisms. We agree with Gower and Simpson (1992) that diffusion creep of coarse-grained quartzo-feldspathic granulites is possible under melt free conditions.

Within the shear zones, Type 2 fabric shows signs of dynamic recrystallization of feldspar by subgrain rotation, increase in aggregate distribution of K-feldspar and decrease in grain size as compared with the coarse-grained Type 1 fabric. The dynamic recrystallization of microperthitic alkaline feldspar occurs via exsolution domain reorganization and subsequent subgrain rotation. Continued recrystallization leads to the development of compositionally discrete populations of new feldspar grains. The extreme ductility of feldspars is caused by high-temperature deformation and probably by high confining pressure. The presence of 'trace element of water' is, according to White and Mawer (1986), crucial for such a behaviour.

The feldspar optical indicatrix orientation of both host and recrystallized grains show a strong preferred orientation, a result of a (010)[100] slip. Quartz c-axes patterns are similar to those of granulites outside shear zones and indicate possible activity of prism-[c] slip. The microstructures and textures of alkali feldspar

suggest that dislocation creep was active in conjunction with stress-controlled intracrystalline diffusion. Interface mechanism-controlled grain boundary sliding is a possible process explaining the extreme ductility of feldspars (White and Mawer, 1986).

Type 3 fabric is characterized by uniform grain-size, a well-equilibrated feldspar microstructure and mineral assemblage (biotite replacing garnets, ilmenite) indicating amphibolite facies retrograde conditions. K-feldspar exhibits extensive microcline twinning that is usually attributed to a decrease in temperature, increase in deformation and/or to an influx of H_2O into the deformed system (Bell and Johnson, 1989). Quartz ribbons are strongly elongated and show signs of intense plastic deformation. The crystallographic preferred orientation of K-feldspar and of quartz is similar to that described previously, and hence indicate activity of the same slip systems. Dislocation creep is probably the dominant mechanism governing the rock flow.

8.2. Structure of granulites

Feldspar in Type 1 fabric is a skeleton-forming mineral with a high degree of contiguity enclosing monomineralic fields of elongated quartz (Fig. 4a). Elongation of quartz and feldspar, high mobility of grain boundaries parallel to the foliation and strong crystallographic fabric of both phases indicate that both minerals were rheologically active but that feldspar was mechanically stronger than quartz. Thus, the rock microstructure can be viewed as a load-bearing framework structure (LBF) marked by a low viscosity contrast between feldspar and quartz (Handy, 1990).

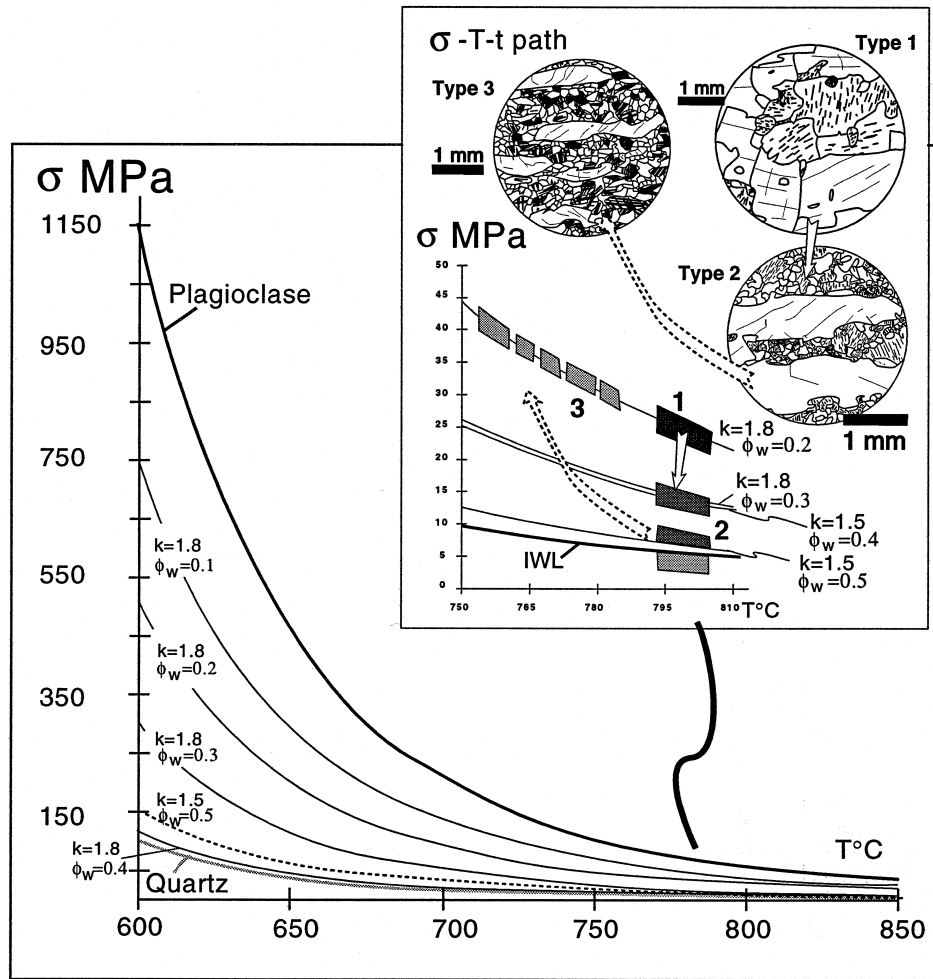The Type 2 fabric (Fig. 4b) resulted from an

Fig. 9. Stress temperature diagram for LBF structure showing the interpretative evolution of creep strength of polyphase plagioclase–quartz aggregates with different amounts of weak phase ϕw (0.1–0.5) and different necking factor k (1.8 and 1.5). Note that at $\phi w = 0.4$ and $k = 1.8$ the strength of polyphase aggregate almost equals that of pure quartz. Upper inset shows tentative $\sigma–T–t$ path of Madagascar granulites coherent with textural evolution of different types of granulites shown in circular insets and changing volume of weak phase and necking factor. Strength curve for IWL structure is marked by a thick line.

increased deformation of coarse-grained granulites in which feldspar recrystallized producing a fine-grained recrystallized matrix. Despite the high strain, quartz does not recrystallize and does not change its grain-size and aspect ratio. This observation suggests that quartz grains were protected from deformation by a weak matrix, that the feldspar matrix did not exert a large shear stress on the quartz grains and that both phases ended up having similar strength. This new microstructure could be viewed either as an LBF structure with high amount of weak matrix composed of two phases of similar viscosity or as an IWL structure where recrystallized feldspar represents a weak phase and relicts of feldspar and quartz grains form strong phases.

The Type 3 fabric (Fig. 4c) is represented by an equigranular feldspar matrix surrounding strongly elongated quartz grains. The grain-size difference

between the feldspar recrystallized in the matrix and quartz is significantly smaller than for Type 2 granulite (Fig. 5). The larger and probably stronger feldspars exerted high shear stress on the weaker quartz, thus forming an LBF structure, but with relatively high viscosity contrast between feldspar and quartz.

Handy (1994) suggested that for small amounts of the weaker phase ($\phi w < 0.1$), the weak phase may never become interconnected and will remain locked within interstitial pockets. Schulmann et al. (1996) have shown that a relatively small volume of quartz (20–30%) in deformed quartzo-feldspathic rocks is contiguous after a relatively small amount of strain at temperatures around 600°C. The Madagascar granulites contain approximately 40% quartz but this phase is not contiguous even if a mineral shape fabric and strong CPO are present. Therefore we need to explain why the quartz in a quartzo-feldspathic granulite does

not form an interconnected phase and why the LBF structure does not collapse into a more stable banded IWL structure of alternating quartz and feldspar layers.

8.3. Stress considerations

K-feldspar and plagioclase exhibit larger strength than quartz (Tullis and Yund, 1977) for all homologous temperatures. In order to show the variations in creep strength with temperature we have calculated values of creep strength σ for albitic plagioclase and quartz (Handy, 1994, equation 5) (Table 1).

The plagioclase experimental creep data were selected because of lack of experimental results for K-feldspar and also because of the similar size and shape of recrystallized plagioclase and K-feldspar grains in studied granulites. Table 1 shows a significant decrease in creep strength for plagioclase and quartz in conjunction with increase in their viscosity ratio with increasing temperature.

The decrease in viscosity ratio between recrystallized feldspar and quartz in Type 2 granulite suggested on the basis of microstructural observations is, therefore, not related to increasing temperature but more likely to a change of deformational mechanisms of feldspar.

By analogy with porous sintered metals, a small amount of a weak phase within a strong phase produces a large degree of weakening relative to the strength of the strong phase (Tharp, 1983). In polyphase materials where the stronger phase is dominant, the bulk strength σ is given by Eudier's formula (Eudier, 1962) modified by Tharp (1983) for rocks

$$\sigma_{\text{rock}} = \sigma_{\text{s}}(1 - k\phi w^{2/3}) \qquad (1)$$

where σ_{rock} is the strength of the porous aggregate and σ_{s} the strength of strong phase, ϕw is the volume proportion of weak phase and k is an experimentally derived factor corresponding to the configuration and the shape of pores. A k value of 0.98 was obtained for perfectly spherical pores with no stress concentrations in necks (Griffith et al., 1979) and 3.8 for elliptical pores with a maximum stress concentration in neck regions. Tharp (1983) estimated empirically a k of 1.8 for porous sintered metals that was also used by Handy (1990, 1994) for the construction of structural stability diagrams. However, in experimentally deformed polyphase rocks the k value is significantly lower and varies between 1.1 and 1.5 (Jordan, 1988). This is explained by the fact that Tharp's value of 1.8 is based on uniaxial tensile tests in which the concentration of stress in neck regions is much higher than in compression tests where the weak phase is also rheologically active.

The low ratio of creep activation energies

$Q_{\text{albite}}/Q_{\text{quartz}}$ (1.5) as well as high ratio of creep exponent $n_{\text{albite}}/n_{\text{quartz}}$ (1.63) expand the stability field of the LBF microstructures to values of ϕw higher than 0.1 (Handy, 1994). Moreover, high-temperature reduces stress concentrations in the neck regions and results in decreasing k.

In order to estimate the influence of the quartz volume in feldspar Type 1 granulite, we have used a modified equation of Rutter and Brodie (1988):

$$\sigma = (1 - k\phi w^{2/3})(\sigma_{\text{plagioclase}} - \sigma_{\text{quartz}}) + \sigma_{\text{quartz}} \qquad (2)$$

We assume that the weak phase volume in Eq. (2) could be taken as 0.3 corresponding approximately to the volume of weak phase (quartz) in granulite. Eq. (2), with $k = 1.8$ and $\phi w = 30\%$ predicts a 75% strength drop from the strength difference between pure albitic rock and rock with 30% of quartz (Fig. 9). Dynamic recrystallization of feldspar in Type 2 fabric leads to the production of a considerable amount of recrystallized K-feldspar–plagioclase matrix that could be considered as a weak phase. The small grain-size of recrystallized feldspar is responsible for a change in deformation mechanisms and a decrease in shear strength at constant temperature (Handy, 1989). On the basis of our microstructural observations, we propose that the recrystallized feldspar may be approximately equally as strong as, or weaker than, quartz during this stage, and we have calculated the amount of weak phase as a sum of quartz and recrystallized feldspar. However, already a 10% increase in recrystallized feldspar will lead to a collapse of the LBF structure for $k = 1.8$.

Therefore, two alternatives can be proposed: (1) an increase in weak phase content due to feldspar recrystallization is related to a decrease in stress concentration in neck zones and hence with a decrease in k. Decreasing k to 1.5 makes the LBF structure stable for a volume of weak fraction of up to 0.5, i.e. 20–30% quartz, and 20–30% recrystallized feldspar; (2) the recrystallized feldspar and quartz grains represent an interconnected weak phase surrounding relics of stronger feldspars (IWL structure), which according to equation 11 of Handy (1994, Fig. 7) promotes significant weakening already for $\phi w = 10\%$. If the recrystallized feldspar and quartz of Type 2 fabric represent interconnected weak layers, than the bulk granulite strength is reduced to 10% that of feldspar and is lower than the strength of the LBF structure for any volume of finely recrystallized feldspar matrix (Fig. 9).

It was already stated that the Type 3 fabric may develop at amphibolite facies conditions and higher H_2O activity. Strongly deformed quartz connected with small difference in average grain size of quartz and feldspar is interpreted as a LBF structure with higher stress concentration in neck zones, consequently

a high $k = 1.8$. This LBF structure is composed of a low amount (30%) weak quartz, $\phi w = 0.3$, and 70% stronger feldspar. Considering temperatures of deformation to correspond to upper amphibolite facies conditions, the strength of the Type 3 fabric should significantly increase with respect to Types 1 and 2 fabrics.

9. Conclusions

The quartzo-feldspathic granulites are the only quartz-rich, highly strained rocks in which 40% quartz does not form an interconnected phase. The lack of its interconnectivity in coarse-grained granulites is explained by diffusion-controlled deformation mechanisms (without presence of melt) and extreme stability of LBF structure at very high temperatures. Dynamic recrystallization of feldpar in conjunction with stress-controlled intracrystalline diffusion is responsible for further decrease in feldspar viscosity. Quartz becomes enveloped by a low viscosity feldspar matrix which inhibits its coalesecence and interconnectivity. Predicted drastic strength decrease in dynamically recrystallized quartzo-feldspathic granulites may provide a realistic basis for stress considerations of deformed lower crust.

Acknowledgements

References

Andriamarofahatra, J., De La Boisse, H., Nicollet, C., 1990. Datation U–Pb sur monazites et zircons du dernier épisode tectono-métamorphique granulitique majeur dans le Sud-Est de Madagascar. Comptes Rendus à l'Académie des Sciences Paris 310, 1643–1648.

Behr, H.-J., 1980. Polyphase shear zones in the granulite belts along the margins of the Bohemian Massif. Journal of Structural Geology 2, 249–256.

Behrmann, J.H., Mainprice, D., 1987. Deformation mechanisms in a high-temperature quartz–feldspar mylonite: evidence for superplastic flow in the lower crust. Tectonophysics 140, 297–305.

Bell, T.H., Johnson, S.E., 1989. The role of deformation partitioning in the deformation and recrystallisation of plagioclase and K-feldspar in the Woodroffe thrust mylonite zone, central Australia. Journal of Metamorphic Geology 7, 151–168.

Besairie, H., 1970. Map Ampanihy, scale 1:500,000. Service géologique de Madagascar.

Blumenfeld, P., Mainprice, D., Bouchez, J.L., 1986. c-Slip in quartz from subsolidus deformed granite. Tectonophysics 127, 97–115.

Bons, P.D., 1993. Experimental deformation of polyphase rock analogues. PhD thesis, University of Utrecht.

Caen-Vachette, M., 1979. Le Précambrien de Madagascar. Radiochronométrie par isochrones Rb/Sr sur roches totales. Revue de Géologie Dynamique et de Géographie Physique 21, 331–338.

Dell'Angelo, L.N., Tullis, J.A., 1988. Experimental deformation of partially melted granitic aggregates. Journal of Metamorphic Geology 6, 495–515.

Eudier, M., 1962. The mechanical properties of sintered low-alloy steels. Powder Metallurgy 9, 278–290.

Flinn, D., 1969. Grain contacts in crystalline rocks. Lithos 2, 361–370.

Gapais, D., Barbarin, B., 1986. Quartz fabric transition in a cooling syntectonic granite (Hermitage Massif, France). Tectonophysics 125, 357–370.

Garbutt, J.M., Teyssier, C., 1991. Prism $\langle c \rangle$ slip in the quartzites of the Oakhurst mylonite belt, California. Journal of Structural Geology 13, 657–666.

Gower, R.J.W., Simpson, C., 1992. Phase boundary mobility in naturally deformed, high-grade quartzo-feldspathic rocks: evidence for diffusional creep. Journal of Structural Geology 14, 301–313.

Griffith, T.J., Davies, R., Basset, M.B., 1979. Analytical study of effects of pore geometry on tensile strength of porous materials. Powder Metallurgy 22, 119–123.

Handy, M.R., 1989. Deformation regimes and the rheological evolution of fault zones in the lithosphere: the effects of pressure, temperature, grain-size and time. Tectonophysics 163, 119–152.

Handy, M.R., 1990. The solid-state flow of polymineralic rocks. Journal of Geophysical Research 95, 8647–8661.

Handy, M.R., 1994. Flow laws for rocks containing two non-linear viscous phases: a phenomenological approach. Journal of Structural Geology 16, 287–301.

Hickey, K.A., Bell, T., 1996. Syn-deformational grain growth: matrix coarsening during foliation development and regional metamorphism rather than static annealing. European Journal of Mineralogy 8, 1351–1373.

Hirth, G., Tullis, J., 1992. Dislocation creep regimes in quartz aggregates. Journal of Structural Geology 14, 145–159.

Jaoul, O., Tullis, J., Kronenberg, A., 1984. The effect of varying water content on the behaviour of Heavitree quartzite. Journal of Geophysical Research 89, 4298–4312.

Ji, S., Mainprice, D., 1988. Natural deformation fabrics of plagioclase: implications for slip systems and seismic anisotropy. Tectonophysics 147, 145–163.

Ji, S., Mainprice, D., Boudier, F., 1988. Sense of shear in high-temperature movement zones from the fabric asymmetry of plagioclase feldspars. Tectonophysics 147, 145–163.

Jordan, P.G., 1987. The deformational behavior of bimineralic limestone–halite aggregates. Tectonophysics 135, 185–197.

Jordan, P.G., 1988. The rheology of polymineralic rocks—an approach. Geologische Rundschau 77, 285–294.

Kretz, R., 1969. On the spatial distribution of crystals in rocks. Lithos 2, 39–66.

Kretz, R., 1994. Metamorphic Crystallisation. Wiley, Chichester.

Kruhl, J.H., 1996. Prism- and basal-plane parallel subgrain boundaries in quartz: a microstructural geothermobarometer. Journal of Metamorphic Geology 14, 581–589.

Lister, G.S., Dornsiepen, U.F., 1982. Fabric transitions in the Saxony granulite terrain. Journal of Structural Geology 4, 81–92.

Mainprice, D., Bouchez, J.-L., Blumenfeld, P., Tubia, J.M., 1986. Dominant c-slip in naturally deformed quartz: implications for dramatic plastic softening at high-temperatures. Geology 14, 819–822.

Martelat, J.E., Nicollet, C., Lardeaux, J.M., Vidal, G., Rakotondrazafy, R., 1997. Lithospheric tectonic structures devel-

oped under high-grade metamorphism in the southern part of Madagascar. Geodinamica Acta 10, 94–114.

McLellan, E.L., 1983. Contrasting textures in metamorphic and anatectic migmatites: an example from the Scottish Caledonides. Journal of Metamorphic Geology 1, 241–262.

Moine, B., Rakotondratsima, C., Cuney, M., 1985. Les pyroxénites à urano-thorianite du Sud-Est de Madagascar: conditions physico-chimiques de la métasomatose. Bulletin de Minéralogie 108, 325–340.

Nicollet, C., 1985. Les gneiss rubanés à cordiérite et grenat d'Ihosy: un marqueur thermobarométrique dans le Sud de Madagascar. Precambrian Research 28, 175–185.

Nicollet, C., 1990. Crustal evolution of the granulites of Madagascar. In: Vielzeuf, D., Vidal, P. (Eds.), Granulites and Crustal Evolution. Kluwer, Dordrecht, pp. 291–310.

Olsen, T., Kohlstedt, D.L., 1984. Analysis of dislocation in some naturally deformed plagioclase feldspars. Physics and Chemistry of Minerals 11, 153–160.

Paquette, J.-L., Nédélec, A., Moine, B., Rakotonddrazafy, M., 1994. U–Pb, Single Zircon Pb-Evaporation, and Sm–Nd Isotopic Study of a granulite domain in SE Madagascar. Journal of Geology 102, 523–538.

Ramsay, J.G., 1967. Folding and Fracturing of Rocks. McGraw-Hill, New York.

Rutter, E.H., Brodie, K., 1988. The role of tectonic grain-size reduction in the rheological stratification of the lithosphere. Geologische Rundschau 77, 295–308.

Sander, B., 1950. Einführung in die Gefügekunde geologischer Körper, zweiter Teil: Die Korngefüge. Springer, Wien.

Schulmann, K., Mlčoch, B., Radek, M., 1996. HT microstructures and rheology of deformed granite, Erzgebirge, Bohemian Massif. Journal of Structural Geology 18, 719–733.

Shackleton, R.M., 1986. Precambrian collision tectonic in Africa. In: Coward, M.P., Ries, A.C. (Eds.), Collision Tectonics, 9. Geological Society Special Publication, pp. 329–349.

Shelton, G., Tullis, J., 1981. Experimental flow laws for crustal rocks. Eos, Transactions American Geophysical Union 62, 396.

Spry, A., 1969. Metamorphic Textures. Pergamon Press, Oxford.

Tharp, T.M., 1983. Analogies between the high-temperature deformation of polyphase rocks and the mechanical behavior of porous powder metal. Tectonophysics 96, T1–T11.

Tullis, J., 1983. Deformation of feldspars. In: Ribbe, P.H. (Ed.), Feldspar Mineralogy. Reviews in Mineralogy, 2. Mineralogical Society of America, pp. 297–323.

Tullis, J., 1990. Experimental studies of deformation mechanisms and microstructures in quartzo-feldspathic rocks. In: Barber, D.J., Meredith, P.G. (Eds.), Deformation Processes in Minerals, Ceramics and Rocks. Unwin Hyman, London, pp. 190–227.

Tullis, J., Yund, R.A., 1977. Experimental deformation of dry Westerly granite. Journal of Geophysical Research 82, 5705–5718.

Urai, J.L., Means, W.D., Lister, G.S., 1986. Dynamic recrystallisation of minerals. In: Hobbs, B.E., Heard, H.C. (Eds.), Mineral and Rock Deformation Laboratory Studies, American Geophysical Union Monograph 36, 161–169.

Vernon, R.H., 1975. Metamorphic Processes: Reactions and Microstructure Development. Wiley, New York.

White, J.C., Mawer, K.M., 1986. Extreme ductility of feldspars from a mylonite, Parry Sound, Canada. Journal of Structural Geology 8, 133–143.

White, S.H., 1976. The effects of strain on the microstructures, fabrics, and deformation mechanisms in quartzites. Philosophical Transactions of the Royal Society of London Series A 283, 69–86.

Windley, B.F., Razafiniparany, A., Razakamanana, T., Ackerman, D., 1994. Tectonic framework of the Precambrian of Madagascar and its Gondwana connections: a review and reappraisal. Geologische Rundschau 83, 642–659.